Proceedings of Proceedings of the ASME 2012 6th International Conference on Energy Sustainability & 10th Fuel Cell Science, Engineering and Technology Conference ESFuelCell2012
July 23-July 26, 2012, San Diego, USA

ESFuelCell2012-91307

DRAFT: OPTIMIZATION OF PURGE CYCLE FOR DEAD-ENDED ANODE FUEL CELL OPERATION

Jixin Chen*
Department of Mechanical Engineering
University of Michigan, Ann Arbor
Michigan 48109
Email: jixinc@umich.edu

Jason B. Siegel
Anna G. Stefanopoulou
Department of Mechanical Engineering
University of Michigan, Ann Arbor
Michigan 48109

ABSTRACT

This paper focuses on the optimization of the purge cycle for dead-ended anode (DEA) operation of a proton exchange membrane (PEM) fuel cell. Controling the purge interval at given operating conditions can optimize the fuel cell efficiency and hydrogen loss during the purge. For this optimization, a model capturing the liquid water and nitrogen accumulation in the anode and the purge flow behavior is presented. A target range of purge interval is then defined based on the minimal purge time that removes the plug of liquid and nitrogen in the channel end and the maximum purge interval beyond which hydrogen is wasted since hydrogen molar fraction all along the channel has been restored to one. If the purge is sufficiently long that all of the accumulated water and nitrogen are removed then the power output in the subsequent cycle (galvanostatic operation) would be highest, compared with incomplete purges which do not fully restore hydrogen concentration in the anode. Such purge schedule, however, is associated with certain amount of hydrogen loss. Therefore, there is a trade-off between hydrogen loss and power output, and a corresponding purge interval that produces the largest efficiency. The optimum purge intervals for different cycle durations are identified. The calculated DEA efficiencies are compared with flow-through (FT) operation. The analysis and model-based optimization methodology presented in this paper can be used for optimizing DEA operation of PEMFC with minimum experimentation and development time.

NOMENCLATURE

- Δt Cycle duration, s
- δt Purge interval, ms
- t_0 Time reference, the end of a DEA cycle and the start of the purge
- t_1 Purge interval to place the hydrogen starvation front at the channel end, referenced to t_0, ms
- t_2 Purge interval to restore the hydrogen in the whole channel with unity molar fraction, referenced to t_0, ms
- i Current density A cm^{-2}
- n Molar fraction
- r Source term in transport equation, mol cm^{-3} s^{-1}
- s Liquid volume fraction
- E Voltage, V
- M Molar mass, Kg mol^{-1}
- N Convective flux, mol cm^{-2} s^{-1}
- J Diffusive flux, mol cm^{-2} s^{-1}
- Q Energy, J
- W Purge flow rate, m^3 s^{-1}

INTRODUCTION

Dead-end anode (DEA) operation was previously proposed and implemented by several groups [1–3]. A DEA fuel cell is fed by dry hydrogen with regulated pressure at the anode inlet. Inlet pressure regulation ensures that the hydrogen inlet stoichiometry is exactly one during DEA operation and the channel pres-

*Address all correspondence to this author.

sure remains constant. A DEA fuel cell system, as shown in Fig.1b, depends on fewer auxiliary components when compared to the more traditional flow-through (FT) mode shown in Fig.1a, which employs hydrogen flow control. The FT operation with hydrogen flow control depends on a recirculation loop to maintain a high hydrogen utilization, which requires hydrogen grade plumbing and hardware such as an ejector/blower, water separator, and hydrogen humidifier. These components add weight, volume, and expense to the system. In DEA operation, the water crossing through the membrane contributes to humidifying the hydrogen fuel so that anode inlet humidification can be removed or reduced.

There are unfortunately other concerns with the DEA fuel cell system. During DEA operation, the nitrogen and liquid water accumulate in the anode channel, causing a gradual drop in cell voltage over time. Purging of the anode channel is necessary to remove the accumulated nitrogen and water before severe voltage drop occurs. A cyclic resetting voltage behavior can be thus observed between two consecutive purges, as illustrated in Fig. 2.

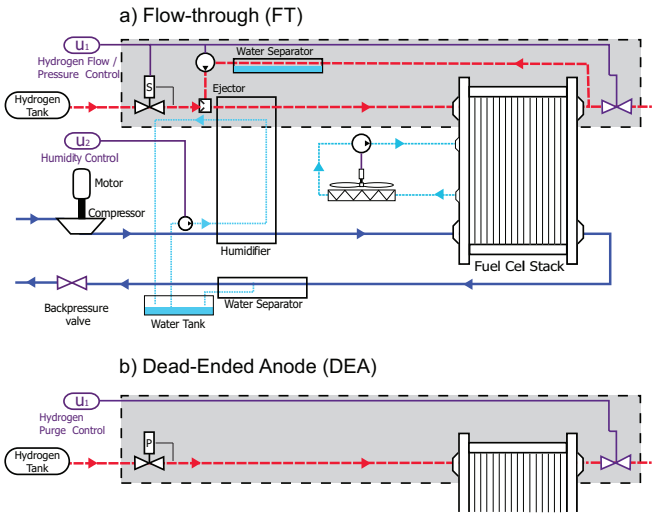

FIGURE 1. Schematic of fuel cell systems with flow-through anode versus dead-ended anode. DEA operation depends on upstream pressure regulation instead of mass flow control. If the purge interval is minimized, there is less need for hydrogen re-circulation and humidification systems.

The accumulation of nitrogen and liquid water in the anode channel during DEA operation may lead to local fuel depletion or starvation, triggering corrosion of the catalyst support carbon in the cathode. Cathode carbon corrosion is a concern because it causes irreversible loss of fuel cell voltage and decreases the stack lifetime. In our recent work [4] the spatio-temporal variable carbon corrosion rate due to the elevated cathode interfacial potential has been studied via simulation. In addition, the uneven local current and membrane water content during DEA operation may accelerate the membrane degradations including membrane crack/tear, pin-hole and polymer decomposition [5, 6]. The impact of degradation on cell terminal voltage and therefore efficiency over the entire lifetime of the cell, is an important consideration for purge scheduling. In a future publication, we hope to elucidate the connection between purge scheduling, degradation and efficiency over the entire cell lifetime.

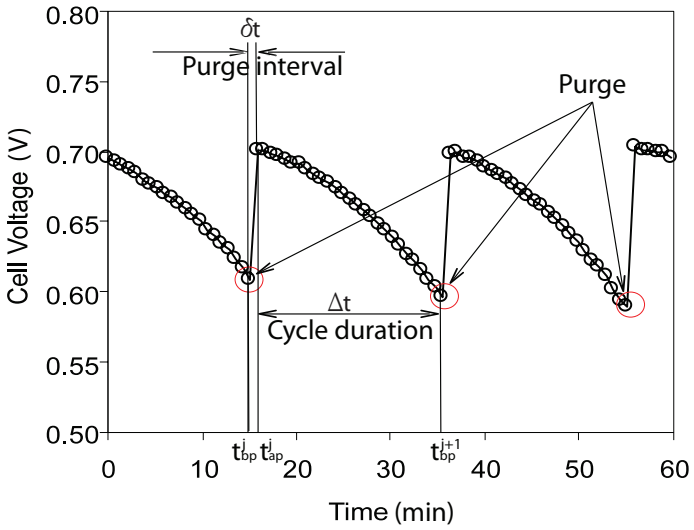

FIGURE 2. Representative voltage cycles during the DEA operation. t_{bp}^{j} is the end of the jth DEA cycle (the moment right before purge) and t_{ap}^{j} is the beginning of the $(j+1)$th cycle (the moment right after purge). Purge interval δt, which equals to t_{ap}^{j+1}-t_{bp}^{j}, is controlled by a solenoid valve downstream of the fuel cell anode. Cycle duration, Δt, is the amount of time between the end of the proceeding purge and the start of the subsequent purge. The accumulation of nitrogen and liquid water in the anode channel between purges is responsible for the recoverable voltage loss in a DEA cycle.

The objective of this paper is to optimize the efficiency of a DEA fuel cell via purge scheduling. The optimization is performed on the purge interval and the cycle duration is considered as an operating parameter. Operating conditions such as current load also influence both fuel cell efficiency and degradation, however for a portable application these conditions are usually determined by the power requirement and thus considered parameters in this study. The optimization is performed based on the simulation results. In the following sections, we will present the along-channel model, then define the target range for purge interval. The purge interval is finally optimized under different cycle durations for achieving the maximum efficiency.

HYDROGEN CONCENTRATION ALONG THE CHANNEL

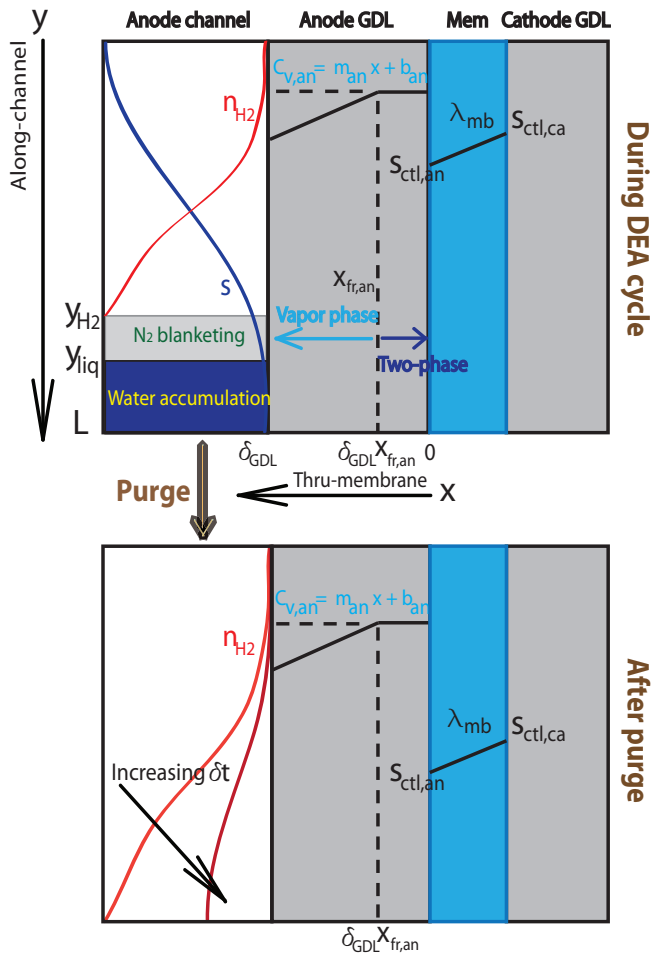

FIGURE 3. A schematic illustrating the modeling domain (not to scale). Species molar fraction (n_i), liquid volume fraction in the channel (s), liquid front in the GDL ($x_{fr,an}$, $x_{fr,ca}$), membrane water content (λ_{mb}) and liquid saturation in the catalyst layer ($s_{ctl,an}$, $s_{ctl,ca}$) are the distributed states along the channel. The liquid water fully occupies the channel when the volume fraction reaches unity. Nitrogen blanketing also contributes to the hydrogen starvation in the channel end. A purge can release the accumulated water and nitrogen, thus restoring the hydrogen concentration in the channel. The GDL states remain unchanged during the purge since the purge interval is in ms scale whereas the cycle duration is in 100 s scale. Increasing purge interval, or more complete purge, leads to higher hydrogen concentration right after the purge.

In previous work [4, 7], we have developed a 1-D (along-channel), single-phase and transient model to study the nitrogen front evolution and associated carbon corrosion in DEA operation. The model predicted spatio-temporal evolutions of species concentration and carbon corrosion rate have been tuned using the gas chromatography [7] and electrode thickness measurement [8]. The physics based model can also predict the cell equilibrium observed during the DEA operation [9].

In this paper we extend our model to capture the liquid water accumulation in the channel end. A model of the channel liquid water is needed because the water impedes the flow of gases during the purge, and longer purge interval is required to clear the channel when liquid is present. A stratified channel distribution with water and nitrogen in the end is expected for a vertical oriented (inlet at the top) DEA cell. As shown in the upper graph of Fig. 3, there is accumulated nitrogen and water in the channel end right before the purge, which leads to local hydrogen starvation and voltage decay. A minimal purge interval is thus to place the hydrogen starvation front (y_{H_2}) right at the channel end, i.e., hydrogen becomes available in the whole channel after the purge without any hydrogen loss during the purge. As illustrated in the lower graph of Fig. 3, with increasing purge interval the hydrogen concentration in the channel becomes higher after the purge, and the power output in the subsequent cycle would be larger, although there is some hydrogen loss during the purge. Finally, a maximum purge interval should exactly and fully restore the hydrogen in the channel, i.e., the hydrogen molar fraction (n_{H_2}) exactly reaches unity in the whole channel, leading to highest power output in the subsequent cycle but greatest amount of hydrogen loss during the purge. These minimal and maximum purge intervals (δt_{min} and δt_{max}) constitute the target range for a purge.

The purge is performed by a solenoid valve at the downstream of the anode outlet. There is physical opening/closing time for the solenoid valve, defined as the time lapse between the solenoid valve energizing/de-energizing and the instant in which the flow at the outlet reaches 90%/10% of its maximum value. Hence, δt_{min} needs to be further constrained by a minimal operating time constant t_{SV} reflecting the physical opening/closing time. In practice, the physical opening/closing time of a solenoid valve is between 0.01 and 0.5 second. Therefore t_{SV} may be larger than δt_{min} or even δt_{max}. The practical target range for purge interval thus becomes [max(t_{SV}, δt_{min}), max(t_{SV}, δt_{max})]. If $t_{SV} > \delta t_{max}$, the purge interval should be always set to t_{SV}. A small value 0.02 s is chosen for t_{SV} in this paper to illustrate the optimization results.

In this case the hydrogen starvation occurs before the purge. However, there exists a special scenario: if the cycle duration becomes shorter then it is possible that hydrogen starvation does not occur even at the channel end, as shown in Fig. 5. Under that circumstance, there would be inevitably certain amount of hydrogen loss during the purge. Therefore the lower limit of the feasible purge interval is always t_{SV}. The target range for purge interval is thus dependent on the cycle duration.

MODEL PRESENTATION

The model inputs are the nominal current I, cathode inlet relative humidity (RH), and cathode stoichiometry ratio (SR). Cell temperature T and Anode(AN)/Cathode(CA) inlet pressures P_{ca}/P_{an}, are fixed parameters in the model but may be adjusted prior to simulation for different experimental conditions. The model outputs are cell voltage, local current density, molar fraction of each species in the anode, membrane water content, anode/cathode liquid saturation in the catalyst layer, liquid water volume fraction in the anode channel, and the liquid front in the anode/cathode GDL. The cell voltage is a scalar quantity while the other outputs represent the vector of distributed values along the channel (y direction) or through the membrane (x direction, only the liquid front, $x_{fr,an}$ and $x_{fr,ca}$). Fig. 3 is a schematic illustrating the modeling domain, the cathode channel not shown for simplicity. In the following, the model is introduced briefly, complete details being available in our future publication at International Journal of Hydrogen Energy.

Gas transport along the channel

In this subsection we present the along-channel transport equations with the consideration of two-phase water behavior. Our prior along-channel transport model framework [4, 7] is extended to capture the local water condensation and accumulation in the anode channel end.

The time dependent composition in the anode is modeled using Stefan-Maxwell equations for a quaternary system (H_2, O_2, N_2, H_2O) and solved by spatial discretization and numerical time integration. The model describes the mass conservation (in both vapor and liquid phases) including convection, diffusion, and source terms in the anode channel:

$$\frac{P_{an}}{RT}\frac{\partial(1-s)n_i}{\partial t} = -\frac{\partial}{\partial y}(J_i + n_i N_t) + r_i \tag{1}$$

for $i = [1,2,3] = [N_2, O_2, Vapor]$, where N_t is the total convective gas flux, J_i is the diffusive flux, and r_i denotes the source terms (reactive and/or crossover fluxes per unit channel height). The volume fraction term, $1-s$, is introduced to account for the change of mass due to the volume change. When s=0, Eq. 1 reduces to the single phase equation of material balance. A similar approach to handle the water phase change in the transport equation can be found in [10, 11]. Only three of the four components are independent in this modeling framework. We choose to model the mole fractions of nitrogen (n_{N_2}), oxygen (n_{O_2}) and water vapor (n_V) as our dynamic states. The anode pressure, P_{an}, is assumed to be constant since it is set by an upstream pressure regulator during the DEA operation.

The causal formulation for the quaternary Stefan-Maxwell diffusive fluxes can be summarized as:

$$J_i = -\frac{P_{AN}}{RT\psi(n)} W \frac{dn_i}{dy} \tag{2}$$

where ψ is a scalar function of the species molar fractions and W is a 4 by 4 coefficient matrix (refer to Ref. [12]).

Assuming the outlet flow is known, $N_t(L) = N_{out}$, then conservation of total mass (gas mixture) allows solving of (1) for $N_t(y)$. Since $\Sigma J_i = 0$ by definition, the equation for mass conservation can be written as:

$$\frac{\partial N_t}{\partial y} = \Sigma r_i \tag{3}$$

N_{out} is zero for DEA operation and assigned a constant value to simulate FT operation and purge flow, then the convective flux along the channel can be found by:

$$N_t(y) = N_t(L) - \int_y^L \big[r_{H_2,rct}(\tilde{y}) + r_{H_2,crs}(\tilde{y}) + r_{N_2,crs}(\tilde{y}) + r_{V,crs}(\tilde{y}) + r_{V,rct}(\tilde{y}) + r_{V,cond}(\tilde{y}) + r_{O_2,crs}(\tilde{y}) + r_{O_2,rct}(\tilde{y}) + \frac{P_{AN}}{RT}\frac{\partial s}{\partial t}\big] d\tilde{y} \tag{4}$$

in which $r_{V,cond}$ denotes the source term due to water condensation. Specifically it can be expressed as:

$$r_{V,cond} = max\big[0, K_{cond}\frac{(n_V P_{AN} - P_{sat})(1-s)}{RT}\big] \tag{5}$$

where P_{sat} is the saturation vapor pressure, K_{cond} is the condensation rate constant in 1/s. The condensation rate is proportional to the difference between the vapor pressure and saturation pressure. The vapor partial pressure is allowed to achieve supersaturation with this model framework. When the vapor pressure is below the saturation pressure, the evaporation effect is not considered for simplicity.

The expressions for other source terms in Eq. 4 are not presented here for brevity, details can be found in [4, 7]. The local current, determined by the species concentration, is the summation of all partial reaction kinetics and a distributed state along the channel. The electrochemical submodel is also not presented here.

Liquid water transport along the channel

In literature, there are two common ways to track the two-phase water transport in the channel and GDL: the multi-phase mixture (M^2) [13] and two-fluid models [11]. In this paper, the

two-fluid approach is used to track the liquid volume fraction along the channel. Rather than calculating the gas phase velocity from the momentum equation, the total gas flux represented by Eq. 4 can be readily converted to velocity, then an interfacial drag coefficient f(s) between liquid and gas phase velocities [11] is used to obtain the liquid phase velocity. Since there is no outlet flow during DEA operation, N_t(L)=0 in Eq. 4, which simplifies the typical two-fluid model framework.

Taking into account diffusion, convection and source term, the liquid water volume fraction is described by the following PDE:

$$\rho_w \frac{\partial s}{\partial t} = \rho_w D_s \frac{\partial^2 s}{\partial y^2} - \rho_w \frac{RT}{P_{AN}} \frac{\partial [f(s) N_t(y)]}{\partial y} + M_w (r_{V,cond} + \frac{N_{l,an}}{d_{ch}}) \tag{6}$$

where ρ_w is the density of water in Kg/m^3, M_w is the molar mass of water in Kg/mol, and D_s is the liquid saturation diffusivity in the channel in m^2/s. There are two contributions to the source term in Eq. 6: $r_{V,cond}$ is the local vapor condensation in the channel and $N_{l,an}$ is the liquid water flux from the GDL to the channel. Detailed expressions can be found in [14]. The convective term drives the liquid water towards the channel end. As the liquid droplets are carried by gas flow, the corresponding interfacial drag coefficient f(s) is assumed as a linear function of liquid water volume fraction [11]:

$$f(s) = K_{slip} s \tag{7}$$

where K_{slip} is the physical velocity slip ratio between liquid and gas, which is a tunable parameter in the model.

Purge flow

The exact amount of flow leaving the channel at the purge event is critical to determine the fuel efficiency and voltage recovery. The purge interval is a parameter to optimize and the volumetric flow rate at the outlet (channel end) is described by [15]:

$$W_{total} = C_{turb} A_{ch} \left[\frac{2}{\rho} \Delta p + (\frac{\nu R_t}{2 C_{turb} D_h})^2 \right]^{0.5} - A_{ch} \nu \frac{R_t}{2 D_h} \tag{8}$$

where C_{turb} = 0.61 is the dimensionless discharge coefficient under turbulence condition, D_h is the hydraulic diameter in m, A_{ch} is the area of the orifice (channel) in m^2, R_t=9.33 is the critical value from [15]; ρ is the density of the mixture flow (liquid water and multiple gas species) in kg/m^3; ν, defined as μ/ρ, is the kinematic viscosity of the mixture flow in m^2/s, and Δp is the differential pressure at the purge. Since the local species molar fraction varies with the channel length and thus purge time, integrating W over the purge interval gives the volumetric displacement of accumulated gas at the channel end.

Because the purge interval is very short (in a scale of ms), the profiles of molar fractions (n_i) and flow rate (W_{total}) at the end of a DEA cycle are assumed to move along the channel direction during the purge without the diffusion effects, which is a typical plug flow behavior.

The density ρ and viscosity ν at the outlet are dependent on the gas composition and liquid volume fraction. The density ρ can be defined by:

$$\rho(y) = (1-s)\rho_g + s\rho_w \tag{9}$$

$$\rho_g(y) = \rho_{N_2} n_{N_2} + \rho_V n_V + \rho_{O_2} n_{O_2} + \rho_{H_2} (1 - n_{N_2} - n_V - n_{O_2}) \tag{10}$$

in which ρ_w is the density of liquid water, and ρ_g is the density of gas mixture. The viscosity is defined similarly. Since the local gas composition varies along the channel, the density/viscosity of the gas mixture is a function of y.

Efficiency of the DEA cell

The DEA cell efficiency would be adversely affected by the amount of hydrogen fuel expelled during the purge. The hydrogen loss during the purge depends on many factors including the anode pressure, temperature, velocity of the flow and the conditions of channel flooding and nitrogen blanketing. The ideal gas law is used to estimate the hydrogen concentration, since the anode pressure and gas temperature are known. Here the gas temperature is assumed to be equal to the cell temperature.

The hydrogen loss in mol at a purge event is calculated by:

$$Q_{loss}^{H_2} = \int_{t_{bp}^j}^{t_{dp}^j} \frac{W_{total}(t,L) n_{H_2}(t,L) P_{AN}}{RT} dt \tag{11}$$

where n_{H_2} is the hydrogen molar fraction at the end of anode channel (y=L). The functional dependence of W_{total}(y=L) on time is implicit, since in Eq. 8 W_{total} is expressed as a function of channel location. The mixture flow is modeled as plug flow, therefore as the purge front moves through the outlet, W_{total}(y=y$'$) is used in Eq. 11, in which $L - y' = \frac{\int W_{total} dt}{d_{ch} w_{ch}}$.

The purge interval can be controlled to achieve $Q_{loss}^{H_2} = 0$, that is, the purge only releases accumulated water and nitrogen at the channel end and it stops when or before the hydrogen front (y_{H_2} in Fig. 3) reaches the channel end.

The total hydrogen consumed during a cycle in mol is simply calculated from the current density setpoint:

$$Q_{rxt}^{H_2} = \frac{iA}{2kF} \Delta t \tag{12}$$

where i is the current density in A cm^{-2}, A is the effective MEA area, k is the number of parallel channels in the anode (k=25) and F is the Faraday constant. Since the purge flow is calculated based on single channel, the hydrogen consumption is also scaled down using the number of anode channels.

The DEA cell efficiency, which considers the hydrogen loss during the purge but excludes the balance of plant (BOP) components, can be described by:

$$\eta = \frac{\frac{1}{k}\int_0^{t_{tot}} E_{cell} i A dt}{\Sigma_1^m \Delta h_f (Q_{rxt}^{H_2} + Q_{loss}^{H_2})} \tag{13}$$

where Δh_f is the enthalpy of formation of hydrogen fuel in J/mol. The cell is operated under galvanostatic condition so that the current is constant. The cell voltage E_{cell} is decreasing with time, therefore integration over a cycle is needed to evaluate the total energy output. The total operating time t_{tot} equals to $m\Delta t$, where m is the number of DEA cycles. By using different m values, one can either evaluate the efficiency from a single cycle and the subsequent purge, or multiple cycles to reflect the influence of cell degradation. In this paper, only a single cycle is evaluated after the system reaches periodic steady state since the degradtion effect is not considered.

If the hydrogen loss is not considered, i.e., $Q_{loss}^{H_2}$=0, Eq. 13 represents the thermodynamic efficiency, that is, the efficiency of the fuel cell eletrochemical conversion.

Eq. 13 can be also used to evaluate the efficiency with FT anode to compare with DEA, in which $\Sigma_1^m Q_{loss}^{H_2}$ is calculated via another way:

$$Q_{loss}^{H_2} = N_t(L) d_{ch} w_{ch} \int_0^{t_{tot}} n_{H_2}(t, L) dt \tag{14}$$

N_t(L) is assigned a positive value rather than zero for FT condition. The anode stoichiometry ratio is thus ($Q_{rxt}^{H_2}$+$Q_{loss}^{H_2}$)/$Q_{rxt}^{H_2}$.

The efficiency defined in Eq. 13 depends on the current setpoint, or the power output in a DEA cycle, which is defined by:

$$P_{DEA} = \frac{1}{\Delta t} \int_{t_{dp}^j}^{t_{bp}^{j+1}} E_{cell} i A dt \tag{15}$$

$\int_{t_{dp}^j}^{t_{bp}^{j+1}} E_{cell} i A dt$ represents the total energy output in a DEA cycle. Both power and energy outputs are defined on the whole cell area rather than scaling it down by the anode channel number.

Table 1 summarizes the parameter values used in the model. There are two steps in implementing the model, the coupled multi-state PDE system representing the DEA cycle is solved first, followed by the purge flow submodel which calculates the hydrogen loss and redistributes all states as the initial condition of the subsequent DEA cycle. The efficiency is evaluated after the system has reached periodic steady state. The coupled PDE system is solved using a variable step solver, Matlab ODE15s, with a relative tolerance of 10^{-4}. The channel is discretized using 51 grids.

RESULTS AND DISCUSSIONS

In this section the simulation results are presented and discussed. First, the model is used to define a target range for the purge interval based on physical considerations to reduce the domain to search. The DEA cell efficiency is then evaluated within the target range and compared with FT efficiency. The influence of cycle duration is also examined.

Target range of purge interval

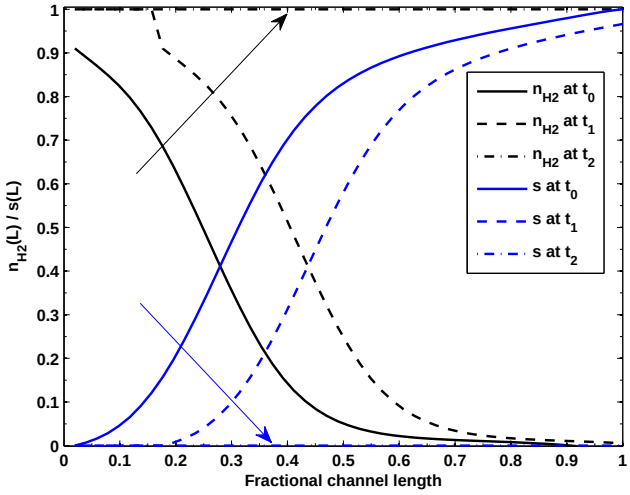

FIGURE 4. Distribution of hydrogen concentration and liquid volume fraction before and after purge. The black curves show the hydrogen molar fraction and the blue ones show the liquid volume fraction. The purge interval should be chosen within the target range defined as follows. A minimal purge interval which places the hydrogen starvation front at the channel end, and a maximum one which exactly and fully restores the hydrogen in the channel without further loss. The simulation results are obtained with the following operating conditions: cycle duration 900 s, current density 0.6 A cm^{-2}, cell temperature 50 °C, cathode RH 0.9, stoichiometry ratio 3 and pressure 1.18 bar.

The DEA operation can minimize or avoid the unnecessary hydrogen loss at the purge with elaborately designed purge

TABLE 1. Geometrical, physical and operating parameters

Quantity	**Value**
Anode inlet pressure P_{AN}	4.5 psig
Cathode systme pressure P_{CA}	4 psig
Cell temperature T	323 K
H_2 enthalpy of formation Δh_f	-242 $\times 10^3$ J/mol
Discharge coefficient C_{turb}	0.61
Critical value for purge flow model R_t	9.33
Anode channel length L	0.0685 m
Anode channel depth d_{ch}	1.78 mm
Anode channel width w_{ch}	2.08 mm
Hydraulic diameter D_h	2.74 mm
Effective MEA area A	50 cm^2
Number of channels k	25
Density of hydrogen ρ_{H_2}	0.0899 kg/m^3
Density of nitrogen ρ_{N_2}	1.25 kg/m^3
Density of vapor ρ_V	0.0835 kg/m^3
Density of oxygen ρ_{O_2}	1.43 kg/m^3
Density of liquid water ρ_w	997 kg/m^3
Viscosity of hydrogen ν_{H_2}	1×10^{-4} m^2/s
Viscosity of nitrogen ν_{N_2}	17.8×10^{-6} m^2/s
Viscosity of vapor ν_V	1.56×10^{-4} m^2/s
Viscosity of oxygen ν_{O_2}	13.99×10^{-6} m^2/s
Viscosity of liquid water ν_w	0.01×10^{-4} m^2/s
Molar mass of water M_w	0.018 Kg/mol
Water condensation rate K_{cond}	1000 1/s
Slip ratio between liquid and gas K_{slip}	0.6
Solenoid valve operating time t_{SV}	0.02 s

scheduling. Fig. 4 is the simulation results illustrating such purge schedule. At the end of the DEA cycle (t=t$_0$), liquid water accumulates in the channel end and completely blocks the channel area when s reaches unity at the end of the channel. The hydrogen concentration reaches zero before the liquid volume fraction reaches unity, meaning that nitrogen blanketing contributes to the hydrogen starvation as well.

In Fig. 4, t$_0$ indicates the end of a DEA cycle and the start of the purge. The minimal purge time, t$_1$, is designed to release the accumulated water/nitrogen and to place the hydrogen starvation front at the channel end. Due to the high purge flowrate (diffusion can be ignored), the profile at t=t$_1$ consists of a shift of the non-starvation hydrogen profile at t=t$_0$ towards the channel end plus a hydrogen restored region (n_{H_2}=1) in the channel inlet. In other words, the purge flow behaves as plug flow. With the minimal purge interval δt$_{min}$=t$_1$−t$_0$, there is no hydrogen loss during the purge, however the hydrogen concentration is low in the channel, which would adversely affect the power output in the subsequent cycle. If the purge is extended to δt$_{max}$ (t$_2$−t$_0$) when the hydrogen molar fraction reaches unity in the whole channel, as indicated by the horizontal line, the power output in the subsequent cycle would be the highest, although there is some hydrogen loss during the purge.

Mathematically, t_1 and t_2 satisfy:

$$L - \int_{t_0}^{t_1} \frac{W_{total}}{w_{ch} d_{ch}} dt = y|_{n_{H_2}=0, t=t_0} \tag{16}$$

$$L - \int_{t_0}^{t_2} \frac{W_{total}}{w_{ch} d_{ch}} dt = 0 \tag{17}$$

Influence of purge interval

In this subsection, the influences of purge interval on the DEA cell efficiency are examined. The model can be used to evaluate the trade-off between hydrogen loss and power output. The simulation results are summarized in Figs. 5-6. Three cases with different cycle durations are examined. As shown in Fig 5, the hydrogen molar fraction decreases when the cycle duration becomes longer, whereas the liquid volume fraction increases. Complete hydrogen starvation is observed only with a long cycle duration (Δt=1100s).

The target range of purge interval depends on the cycle duration, since it determines the end-of-cycle (t$_{bp}$) species distribution and the purge flow rate. In Fig. 6, the ranges of purge interval presented for each curve are different as the simulation is only performed within the target range of that design variable. The lower limit of δt is t$_{SV}$ for all cases, which means that either the hydrogen starvation does not occur even at the channel end (Δt=500 and 800s), or t$_{SV}$ >δt$_{min}$ ($\Delta t = 1100s$). Physically, t$_{SV}$ > δt$_{min}$ indicates that there is still hydrogen loss from t$_1$ to t$_0$+t$_{SV}$ after y$_{H_2}$ reaches the channel end.

The hydrogen molar fraction at the channel end increases with purge interval and eventually reaches unity at purge interval δt$_{max}$ as shown in the first subplot of Fig. 6. The second to

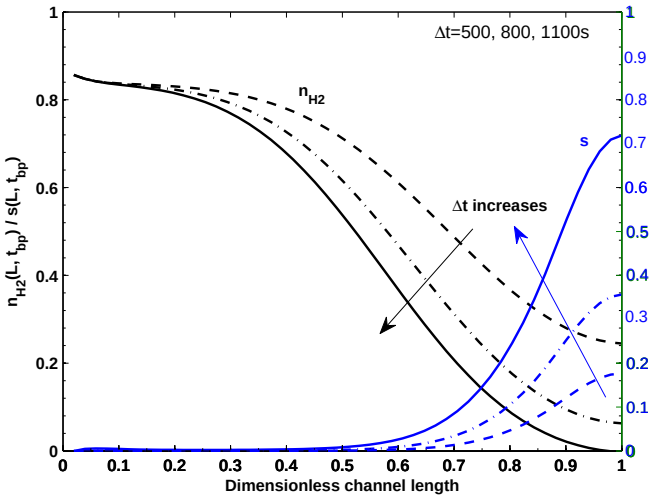

FIGURE 5. The along-channel distribution of hydrogen molar fraction (black) and liquid volume fraction (blue) at the end of a DEA cycle for three different cycle durations. The operating conditions are: current density 0.4 A cm^{-2}, cell temperature 50 °C, cathode RH 100%, stoichiometry ratio 3 and pressure 1.18 bar. The hydrogen starvation is observed in the channel end region when the cycle duration increases to 1100s.

TABLE 2. Summary of FT efficiency

N_{out}, mol cm$^{-2}s^{-1}$	η	SR	Energy, KJ	Power, W
1×10^{-6}	0.5410	1.0082	17.65	16.04
5×10^{-6}	0.5237	1.0416	17.67	16.06
10×10^{-6}	0.5029	1.0846	17.69	16.08

fourth subplots indicate that an extended purge indeed leads to larger power output since the hydrogen concentration is higher during the subsequent DEA cycle. On the other hand, it would produce larger amount of hydrogen loss, as shown in the fifth subplot. These two factors apply opposite influences on the efficiency (Eq. 13), and the more dominant one becomes apparent according to the last subplot.

The calculated efficiencies do not show substantial differences ($<$ 2%), because the purge interval is already constrained in the target range. This suggests that as long as the purge interval lies within the target range, then its influences on the efficiency may be negligible when there are more sensitive design variables involved. For the cases with Δt=500 and 800s, increasing purge interval leads to lower cell efficiency. However, when the cycle duration increases to 1100s, longer purge interval is preferred until a maximum efficiency of 52.9% is reached, after

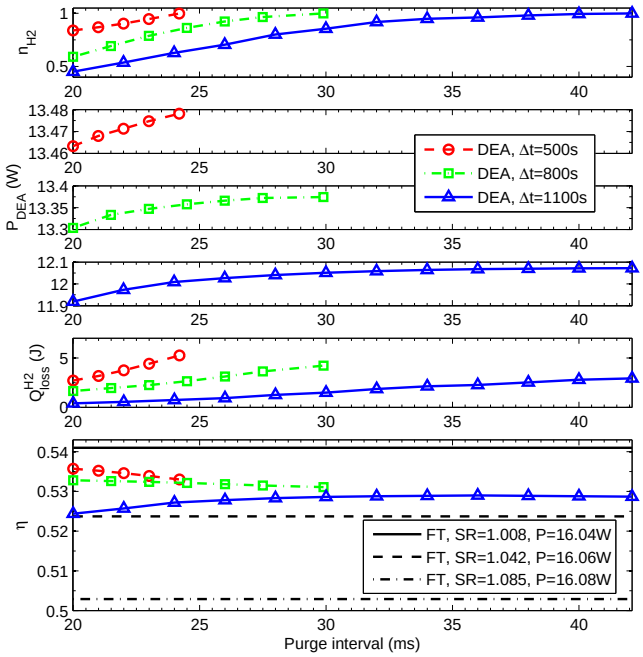

FIGURE 6. The influences of purge interval and cycle duration, with operating conditions being: current density 0.4 A cm^{-2}, cell temperature 50 °C, cathode RH 100%, stoichiometry ratio 3 and pressure 1.18 bar. The simulation results are collected after the system reaches periodic steady state. The three colored curves with markers represent the simulation results obtained from three different cycle durations. The x-limits of each curve indicate δt_{min} and δt_{max} for that cycle duration. The first subplot shows the hydrogen molar fraction at the channel end after the purge. The second to fourth subplots present the power outputs in the subsequent cycle after the purge. The fifth subplot indicates the hydrogen loss during the purge with different purge intervals. Finally, the sixth subplot compares the efficiencies of the DEA operation with different purge intervals and that of the FT operation. The black horizontal lines represent the FT efficiencies calculated with different anode stoichiometry ratio, i.e., different constants assigned to N_{out} (see Table 2).

which the efficiency slightly decreases. These findings indicate that if complete hydrogen starvation has not been observed in the channel end, reducing the hydrogen loss is more significant than restoring the hydrogen concentration in the anode. Even with complete hydrogen starvation (Δt=1100), δt=36 ms, rather than δt_{max}=42.1 ms, gives the largest efficiency.

The flow through efficiencies with different anode stoichiometry ratios are co-plotted for comparison. Only when the stoichiometry ratio is small (1.008), the FT operation gives larger efficiency over DEA. With higher stoichiometry ratios the FT ef-

ficiencies drop rapidly and become smaller than all DEA cases as shown in Table 2 the last subplot of Fig. 6.

The duration to evaluate FT operation is 1100 s in Table 2 and the operating conditions are the same with those in Fig. 6. A higher N_{out} value corresponds to a larger amount of un-reacted hydrogen fuel that leaves the channel. The total energy output is calculated by $\int_0^{t_{tot}} E_{cell} i A dt$. The higher N_{out}, or higher stoichiometry ratio, leads to limited boost of energy or power output, however the loss due to un-reacted hydrogen increases more quickly. Therefore the efficiency drops with increasing N_{out} values.

The present analysis is based on identical cycle number (one cycle), rather than total operating time, to evaluate and compare the efficiencies. The degradation over multiple DEA cycles has not been considered, also, only the fuel cell is considered without the BOP components in the system. For example, the anode humidifier required for flow through operation would consume additional parasitic power. Thus the findings could be different when these factors are considered.

CONCLUSIONS

In this paper, we focus on the optimization of purge interval in order to achieve the maximum DEA fuel cell efficiency. We extended our along-channel, single-phase and transient model to capture the liquid water accumulation in the anode channel end and the purge flow behavior. A target range for purge interval is defined based on the minimal purge time that removes the plug of liquid and nitrogen in the channel end and the maximum purge interval beyond which hydrogen is wasted since hydrogen molar fraction all along the channel has been restored to one. A systematic way to study the DEA cell efficiency is also presented. Using simulations we investigated the influences of purge interval on the power output in the subsequent cycle, the hydrogen loss during the purge, and finally the total efficiency of the DEA cell. At the operating conditions of 0.4 A cm^{-2}, cell temperature 50 °C, cathode RH 100% and pressure 1.18 bar, it is found that shorter purge with less hydrogen loss is preferred if Δt=500, 800s, whereas there exists a maximum efficiency of 52.9% if Δt=1100s when the purge interval (36 ms) is less than the maximum feasible one (42.1 ms). When there is not severe hydrogen starvation in the anode channel end, reducing hydrogen loss (a shorter purge interval) is more important than fully restoring the hydrogen concentration. As long as the purge interval is chosen from the target range, the variation of efficiency due to purge interval is limited. The flow-through operation shows better efficiency over DEA only when the stoichiometry ratio is small (1.008). In future work, the cycle duration will be considered as another design variable relevant to the durability, and the optimization will be performed over a 2-D domain. The influences of carbon corrosion on the power output and cell efficiency during multiple DEA cycles will be studied in details.

ACKNOWLEDGMENT

This work is funded by the National Science Foundation through CBET-0932509 and Ford Motor Company.

REFERENCES

[1] Mocoteguy, P., Druart, F., Bultel, Y., Besse, S., and Rakotondrainibe, A., 2007. "Monodimensional modeling and experimental study of the dynamic behavior of proton exchange membrane fuel cell stack operating in dead-end mode". *Journal of Power Sources*, ***167***, pp. 349–357.

[2] McKay, D., Siegel, J., Ott, W., and Stefanopoulou, A., 2008. "Parameterization and prediction of temporal fuel cell voltage behavior during flooding and drying conditions". *Journal of Power Sources*, ***178***, pp. 207–222.

[3] Siegel, J., McKay, D., Stefanopoulou, A., Hussey, D., and Jacobson, D., 2008. "Measurement of liquid water accumulation in a PEMFC with dead-ended anode". *Journal of Electrochemical Society*, ***155***, pp. B1168–B1178.

[4] Chen, J., Siegel, J. B., Matsuura, T., and Stefanopoulou, A. G., 2011. "Carbon corrosion in PEM fuel cell dead-ended anode operations". *Journal of Electrochemical Society*, ***158***, pp. B1164–B1174.

[5] Curtin, D., Lousenberg, R., Henry, T., Tangeman, P., and Tisack, M., 2004. "Advanced materials for improved PEMFC performance and life". *Journal of Power Sources*, ***131***, pp. 41–48.

[6] Mittal, V., Kunz, H., and Fenton, J., 2007. "Membrane degradation mechanisms in PEMFCs". *Journal of Electrochemical Society*, ***154***, pp. B652–B656.

[7] Siegel, J., Bohac, S., Stefanopoulou, A., and Yesilyurt, S., 2010. "Nitrogen front evolution in purged polymer electrolyte membrane fuel cell with dead-ended anode". *Journal of Electrochemical Society*, ***157***, pp. B1081–B1093.

[8] Matsuura, T., Siegel, J., Chen, J., and Stefanopoulou, A., Washington D.C., 2011. "Multiple degradation phenomena in polymer electrolyte fuel cell operation with dead-ended anode". *Proceeding of ASME 2011 5th International Conference on Energy Sustainability & 9th Fuel Cell Science, Engineering and Technology Conference*.

[9] Chen, J., Siegel, J. B., and Stefanopoulou, A. G., San Francisco, CA, 2011. "Nitrogen blanketing front equilibria in dead end anode fuel cell operation". In American Control Conference.

[10] Jiao, K., and Li, X., 2009. "Three-dimensional multiphase modeling of cold start processes in polymer electrolyte membrane fuel cells". *Electrochimica Acta*, ***54***, pp. 6876–6891.

[11] Ye, Q., and Nguyen, T., 2007. "Three-dimensional simulation of liquid water distribution in a PEMFC with experimentally measured capillary functions". *Journal of Electrochemical Society*, ***154***, pp. B1242–B1251.

[12] Amundson, N. R., Pan, T.-W., and Paulsen, V. I., 2003. "Diffusion with Stefan and Maxwell". *AIChE Journal,* ***49***, pp. 813–830.

[13] Wang, Y., and Wang, C.-Y., 2005. "Modeling polymer electrolyte fuel cells with large density and velocity changes". *Journal of Electrochemical Society,* ***152***, pp. A445–A453.

[14] Siegel, J., Stefanopoulou, A., Ripaccioli, G., and Di Cairano, S., 2010. "Purge Scheduling for Dead-Ended Anode Operation of PEM Fuel Cells," to appear in *The Control Handbook, Second Edition: Control System Applications, Second Edition* . CRC Press.

[15] Borutzky, W., Barnard, B., and Thoma, J., 2002. "An orifice flow model for laminar and turbulent conditions". *Simulation modeling practice and theory,* ***10***, pp. 141–152.